Supporting Information

A colorimetric immunoassay based on coordination polymer composite for the detection of carcinoembryonic antigen

Sixuan Wu, Hongliang Tan*, Caihong Wang, Jinhong Wang, Shouri Sheng*

Key laboratory of Chemical Biology of Jiangxi Province, College of Chemistry and Chemical Engineering, Jiangxi Normal University, Nanchang, 330022, China

* E-mail: hltan@jxnu.edu.cn (H. Tan)

shengsr@jxnu.edu.cn (S. Sheng)

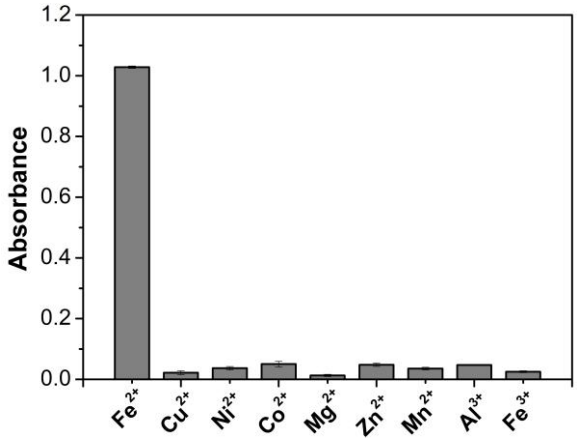

Figure S1. Absorbance responses of Phen solution to different metal ions (each 0.8 mM).

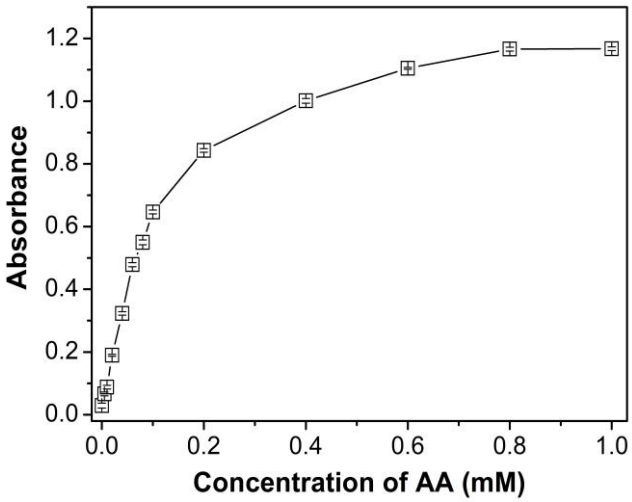

Figure S2. Absorbance of the Phen-Fe^{3+} solution in the presence of AA with different concentrations.

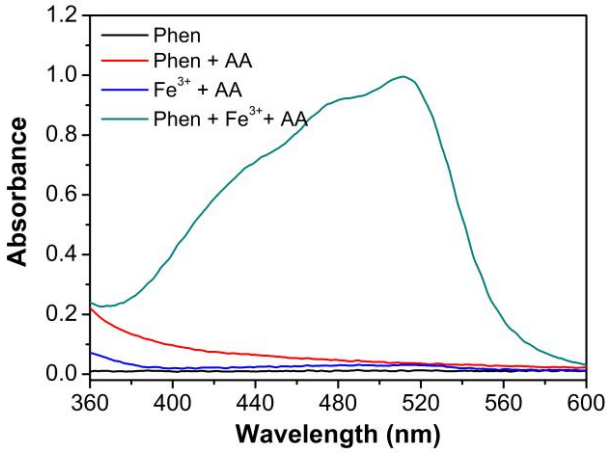

Figure S3. Absorption spectra of the solutions of Phen, Phen + AA, Fe^{3+} + AA, and Phen + Fe^{3+}+ AA.

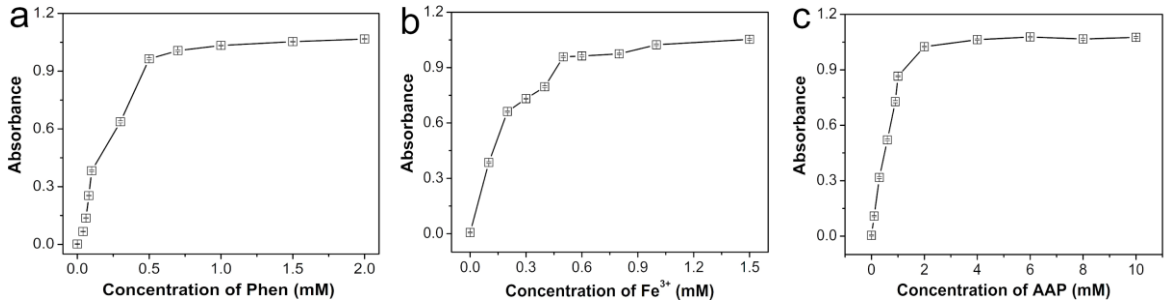

Figure S4. Absorbance intensity of $[(Phen)_3Fe]^{2+}$ complex at 510 nm under different conditions. (a) The concentration of Fe^{3+} and AAP are fixed at 0.5 and 2 mM, respectively, while Phen concentration is varied. (b) The concentration of Phen and AAP are fixed at 0.5 and 2 mM, respectively, while Fe^{3+} concentration is varied. (c) The concentration of Fe^{3+} and Phen are both at 0.5 mM, while AAP concentration is varied.

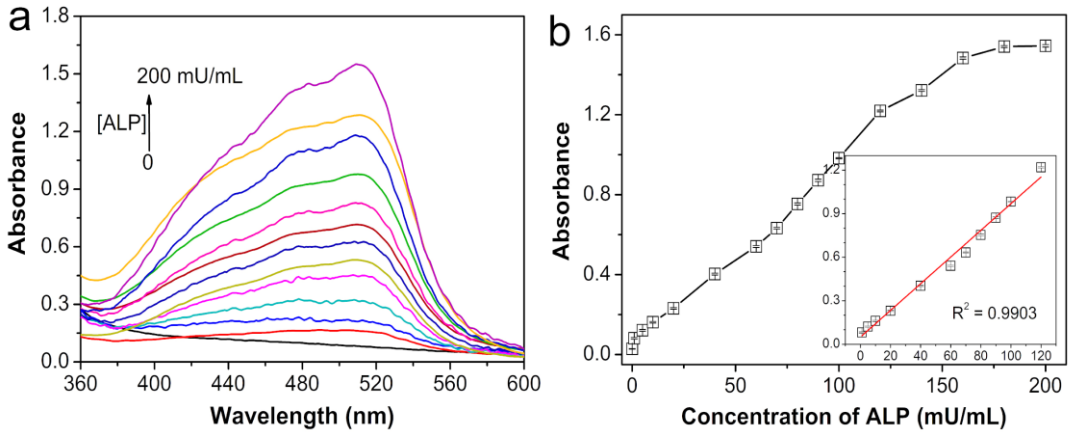

Figure S5. Absorption spectra (a) and intensity at 510 nm (b) of the Phen-Fe^{3+} solution in the presence of 2 mM of AAP and ALP with different concentrations. Inset is the calibration curve of the absorbance of $[(Phen)_3Fe]^{2+}$ complex at 510 nm versus ALP concentration.

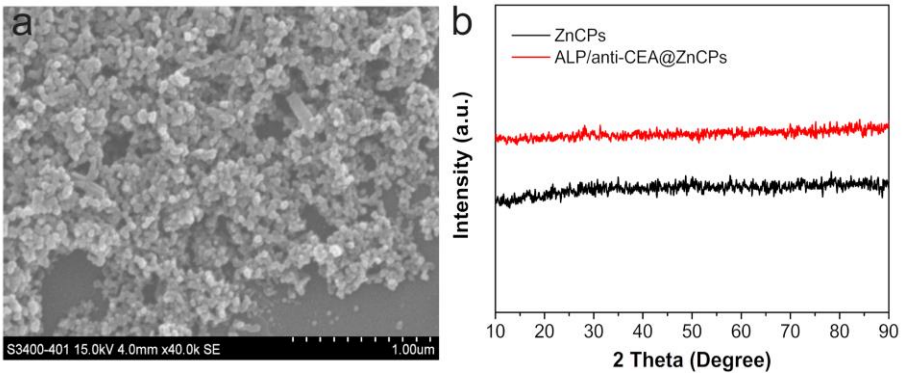

Figure S6. (a) SEM image of ZnCPs. (b) Powder XRD patterns of ZnCPs and ALP/anti-CEA@ZnCPs.

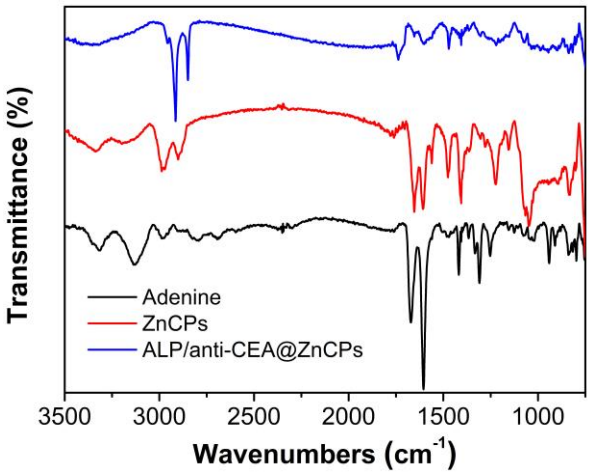

Figure S7. FTIR spectra of adenine, ZnCPs and ALP/anti-CEA@ZnCPs.

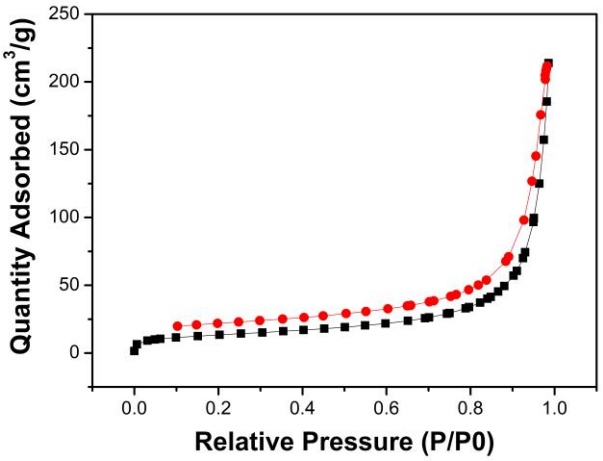

Figure S8. N_2 adsorption-desorption isotherms of ZnCPs.

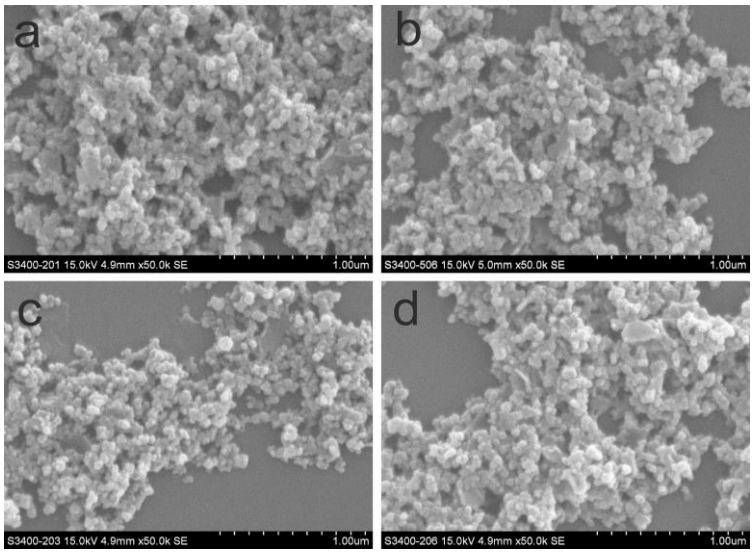

Figure S9. SEM images of ZnCPs after keeping in aqueous solution for different times (from a to d: 0, 1, 3, 7 days).

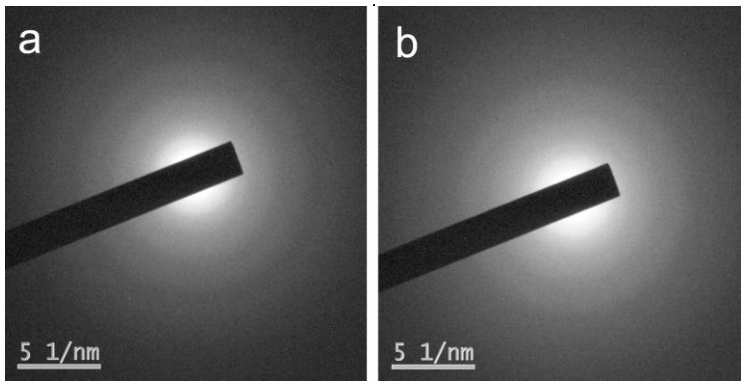

Figure S10. Selected area electron diffraction images of ZnCPs (a) and ALP/anti-CEA@ZnCPs (b).

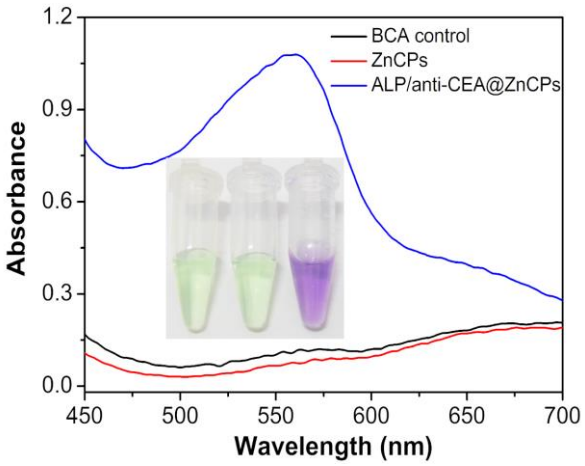

Figure S11. BCA assay of ZnCPs and ALP/anti-CEA@ZnCPs.

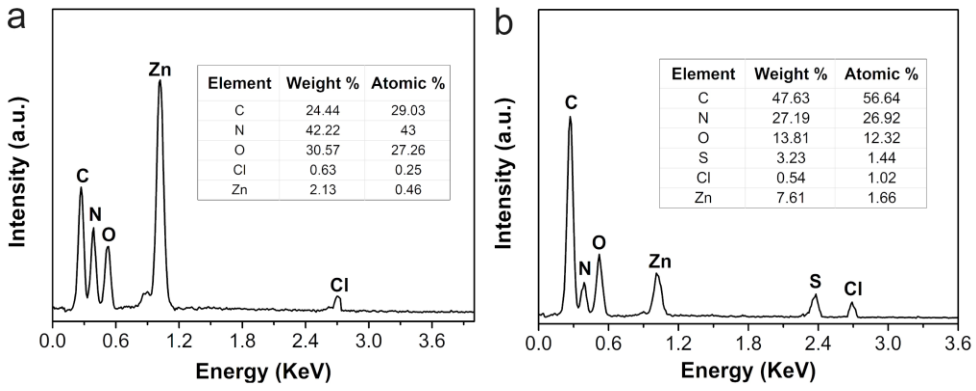

Figure S12. EDS spectra of ZnCPs (a) and ALP/anti-CEA@ZnCPs (b).

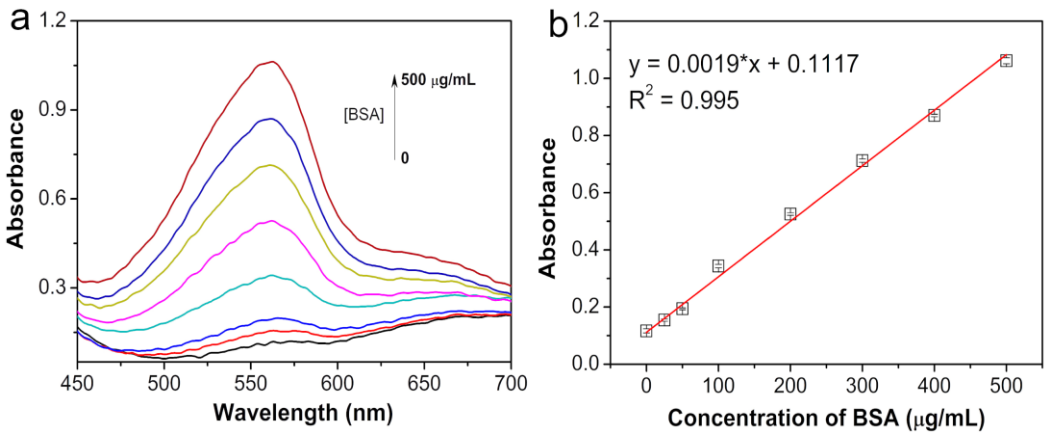

Figure S13. (a) Absorbance spectra of BCA reagent in the presence of bovine serum albumin (BSA) with concentration from 0 to 500 μg/mL. (b) The calibration curve of the absorbance of BCA reagent at 650 nm as a function of BSA concentrations.

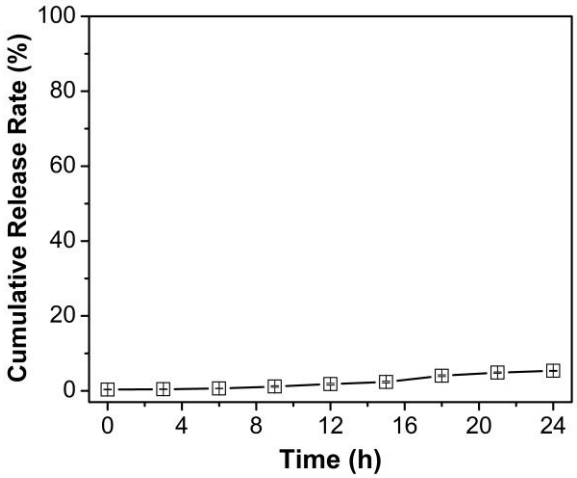

Figure S14. Proteins release profile from ALP/anti-CEA@ZnCPs in ultrapure water.

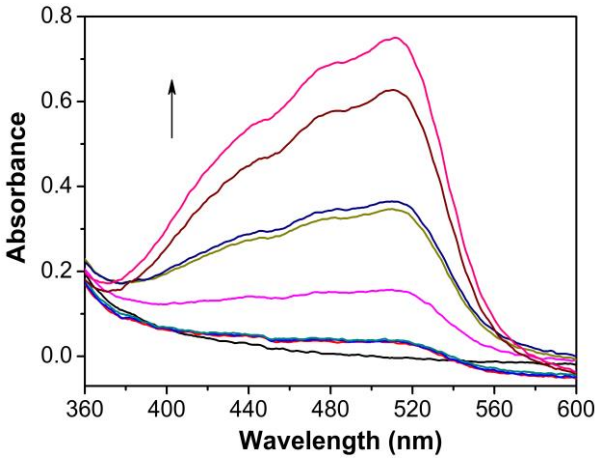

Figure S15. Absorption spectra of Phen-Fe^{3+} solution in the presence of AAP (2 mM) and ALP/anti-CEA@ZnCPs with different amounts (from 0 to 100 μg).

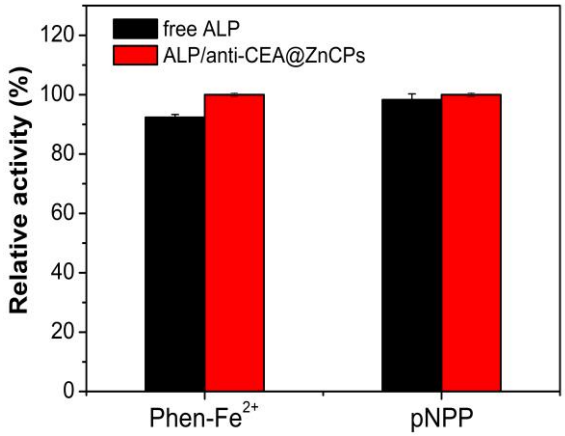

Figure S16. Relative activities of free ALP and ALP/anti-CEA@ZnCPs obtained from substrate systems of pNPP and the mixture of Phen and Fe^{2+} (Phen-Fe^{2+}).

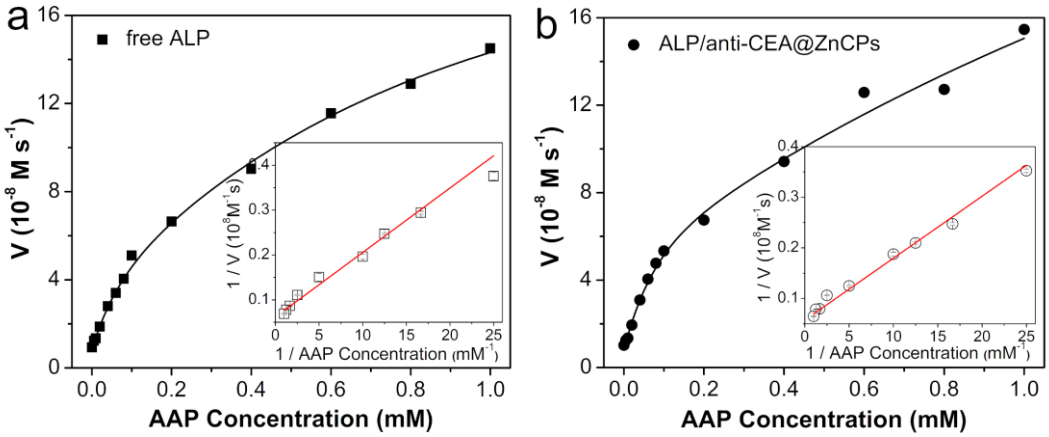

Figure S17. (a) Steady-state kinetic assays of free ALP (a) and ALP/anti-CEA@ZnCPs (b) in the presence of AAP with different concentrations. The insets are their corresponding double-reciprocal plots.

The kinetic behaviors of free ALP and ALP/anti-CEA@ZnCPs were studied by monitoring the absorbance of $[(Phen)_3Fe]^{2+}$ complex in 3-min intervals while varying the AAP concentration. The Michaelis-Menten constant was calculated by using Lineweaver-Burk plots of the double reciprocal of the Michaelis-Menten equation, $1/v = K_m/V_m\,(1/[S] + 1/K_m)$, where v is the initial velocity, V_m represents the maximal reaction velocity, [S] corresponds to the substrate concentration, and K_m is the Michaelis constant.

Table S1. Kinetic data for free ALP and ALP/anti-CEA@ZnCPs

Catalyst	K_m (mM)	V_{max} (10^{-8} M s^{-1})	K_{cat} (s^{-1})
free ALP	0.15	7.53	68.45
ALP/anti-CEA@ZnCPs	0.12	8.05	73.18

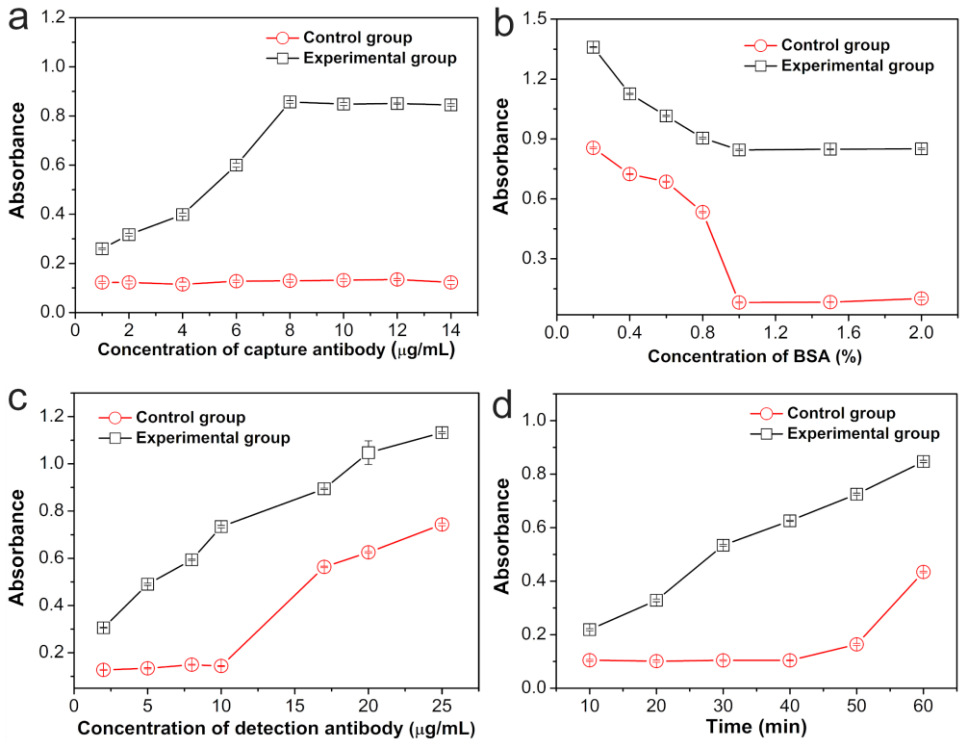

Figure S18. Effects of the concentration of capture antibody (a), blocking agent (b), ALP/anti-CEA@ZnCPs (c), and reaction time (d) on ALP/anti-CEA@ZnCPs-based immunoassays with (red, as experimental group) and without (black, as control group) antigens.

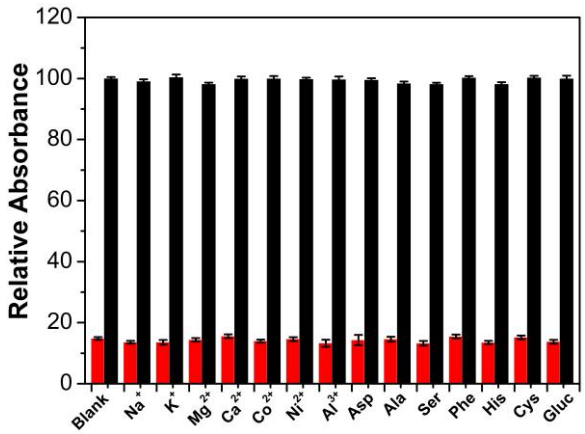

Figure S19. Effects of metal ions and biological species on the colorimetric immunoassay based on ALP/anti-CEA@ZnCPs as a detection antibody. Black bars represent the addition of single interfering material (100 μM). Red bars represent the addition of the mixture of CEA (100 ng/mL) and interfering materials (100 μM).

Table S2. Comparison of various immunoassays for CEA detection.

Antibody labels	Readout signal	Linear range (ng/mL)	LOD (pg/mL)	Ref.
Gold nanoparticle	Colorimetric	0.05 - 50	48	1
Nanogold/graphene	Electrochemical	0.05 - 350	10	2
HRP	Electrochemical	0.5 - 167	100	3
AuNP	Chemiluminescence	5 - 20	100	4
Eu^{3+}	Fluorescence	1 - 1000	500	5
ZnO/GOx-graphene	Electrochemiluminescence	0.01 - 80	3.3	6
Ag@Au nanoparticle	Dynamic light scattering	0.06 - 50	35.6	7
ALP/anti-CEA@ZnCPs	Colorimetric	0.05 - 100	21.1	This work

Table S3. Determination of CEA in human sample

Added (ng/mL)	Detected (ng/mL)	Recovery (%)	RSD (n =3, %)	Kit assay (ng/mL)
20	19.98	99.9	1.24	20.01
40	40.27	100.67	0.32	40.13
60	61.66	102.76	0.56	59.87
80	76.33	95.41	0.37	79.73

Calculation of detection limit

The detection limit was calculated according to previous reports.[8-9] The absorbance signals of the blank sample (without target CEA) were executed with three repeated experiments, which exhibits an average absorbance signal (I_{blank}) of 1.00 and a standard deviation (SD) of 0.5269. With a signal-to-noise ratio of 3, the minimum detectable signal (A) could be calculated as $A = I_{blank} + 3SD = 2.5809$. The value of 2.5809 was then inserted into the linear equation ($y = 0.1451x + 2.5778$). On this basis, the LOD was finally calculated to be 21.1pg/mL.

References

1. Liu, M.; Jia, C.; Jin, Q.; Lou, X.; Yao, S.; Xiang, J.; Zhao, J., Novel Colorimetric Enzyme Immunoassay for the Detection of Carcinoembryonic Antigen. *Talanta* **2010,** *81*, 1625-1629.
2. Zhong, Z.; Wu, W.; Wang, D.; Wang, D.; Shan, J.; Qing, Y.; Zhang, Z., Nanogold-Enwrapped Graphene Nanocomposites as Trace Labels for Sensitivity Enhancement of Electrochemical Immunosensors in Clinical Immunoassays: Carcinoembryonic Antigen as a Model. *Biosens. Bioelectron.* **2010,** *25*, 2379-2383.
3. Dai, Z.; Yan, F.; Yu, H.; Hu, X.; Ju, H., Novel Amperometric Immunosensor for Rapid Separation-Free Immunoassay of Carcinoembryonic Antigen. *J. Immunol. Methods* **2004,** *287*, 13-20.
4. Yang, X.; Guo, Y.; Wang, A., Luminol/Antibody Labeled Gold Nanoparticles for Chemiluminescence Immunoassay of Carcinoembryonic Antigen. *Anal. Chim. Acta* **2010,** *666*, 91-96.
5. Hou, J.-Y.; Liu, T.-C.; Lin, G.-F.; Li, Z.-X.; Zou, L.-P.; Li, M.; Wu, Y.-S., Development of an Immunomagnetic Bead-Based Time-Resolved Fluorescence Immunoassay for Rapid Determination of Levels of Carcinoembryonic Antigen in Human Serum. *Anal. Chim. Acta* **2012,** *734*, 93-98.
6. Cheng, Y.; Yuan, R.; Chai, Y.; Niu, H.; Cao, Y.; Liu, H.; Bai, L.; Yuan, Y., Highly Sensitive Luminol Electrochemiluminescence Immunosensor Based On ZnO Nanoparticles and Glucose Oxidase Decorated Graphene for Cancer Biomarker Detection. *Anal. Chim. Acta* **2012,** *745*, 137-142.
7. Miao, X.; Zou, S.; Zhang, H.; Ling, L., Highly Sensitive Carcinoembryonic Antigen Detection Using Ag@Au Core-Shell Nanoparticles and Dynamic Light Scattering. *Sens. Actuators B-Chem.* **2014,** *191*, 396-400.
8. Long, G. L.; Winefordner, J. D., Limit of Detection. A Closer Look at the IUPAC Definition. *Anal. Chem.* **1983,** *55*, 712A-724A.
9. Chen, A.; Ma, S.; Zhuo, Y.; Chai, Y.; Yuan, R., In Situ Electrochemical Generation of Electrochemiluminescent Silver Naonoclusters on Target-Cycling Synchronized Rolling Circle Amplification Platform for MicroRNA Detection. *Anal. Chem.* **2016,** *88*, 3203-3210.